Predictability of self-organizing systems

S. L. Pepke and J. M. Carlson
Department of Physics, University of California, Santa Barbara, California 93106
(Received 13 December 1993; revised manuscript received 17 March 1994)

We study the predictability of large events in self-organizing systems. We focus on a set of models which have been studied as analogs of earthquake faults and fault systems, and apply methods based on techniques which are of current interest in seismology. In all cases we find detectable correlations between precursory smaller events and the large events we aim to forecast, though in some cases the correlations are very weak. We compare predictions based on different patterns of precursory events and find that for all of the models a precursor based on the spatial distribution of activity outperforms more traditional measures based on temporal variations in the local activity.

PACS number(s): 05.45.+b, 91.30.Px, 02.50.−r, 05.20.−y

I. INTRODUCTION

Self-organized criticality (SOC) has received considerable attention over the past several years, as a possible means to explain scaling behaviors observed in a broad class of nonequilibrium systems including systems in geology, economics, and biology [1]. The theoretical prototype is the sandpile model, in which sand is slowly added to a pile and released in instantaneous avalanches of a wide range of sizes which are triggered when the height (or slope or stress) locally exceeds a specified threshold. Self-organized criticality refers to the particular case of when the system size sets the cutoff for the largest events which are observed. More generally, self-organizing systems, whether critical or not, typically exhibit scaling over some range of sizes and are thought to evolve so that fluctuations in space and time are intrinsically coupled by an underlying threshold dynamics. There has recently been a considerable effort to use self-organizing systems as simple dynamical models of seismic phenomena [1–4] in part due to the clear connection between earthquakes and threshold dynamics. Particular attention has been paid to the robust power-law scaling relation—the Gutenberg-Richter law [5]—relating the frequency of earthquakes to their size.

An alternative direction of research concerns the predictability of the systems, which has important practical applications. The basic approach in such an endeavor is to utilize the available history of the system to forecast future events. Often one is most interested in predicting the largest events (e.g., great earthquakes), and it is the largest events with which we will be concerned here. Of course, in a well defined deterministic system precise knowledge about the present configuration of the system will yield very good, if not perfect, prediction. However, for many real systems specific equations describing the detailed evolutions of the system are not known, and, in addition, the information on which the forecast must be based is typically incomplete. The basic prediction problem is, therefore, an inverse problem in the sense that one wants to use some information such as the time series of events to infer something about the likely phase space trajectory of the system which is, in most practical situations, completely inaccessible to measurement.

For example, earthquake catalogs list the date, time, location, and magnitude of detected events and thus provide one possible source from which one might hope to deduce information about local stresses on a fault. If correlations are detected, they may lead to measurable precursors that are useful for forecasting. While certain seismicity patterns have been recorded in catalogs prior to some subset of the large earthquakes, in most cases the catalogs are too short to determine conclusively whether there is a statistically significant correlation between these patterns and large events. Dynamical models of earthquake faults can thus be particularly useful in the context of the prediction problem. Study of models allows us to consider catalogs of arbitrary size, from which we can make statistically significant statements about both the intrinsic predictability of dynamical systems of this type and the value of current prediction algorithms.

In this paper we address prediction issues in a variety of self-organizing systems. The algorithms that we use are similar to, and clearly motivated by, the work of Keilis-Borok and Kossobokov [6], which we describe briefly below. Our motivations for applying prediction algorithms to a broad class of systems is to try to acertain what classes of precursory phenomena are consistently observed in all of the models. The point here is that no completely realistic dynamical model of faults presently exists, but if the real system resembles in any substantive way the threshold dynamics characteristic of the models, then precursors which are observed in a broad class of models may prove useful in real systems. In the course of this endeavor we develop an alternative type of precursor that is currently not in use in any form in the seismology community, which performs particularly well in the models. In addition, an unanticipated result from our simulations is that the degree of predictability in different systems can differ quite significantly, and that for the systems we have considered those which have no apparent conservation law seem to be more predictable than those with a conservation law. Finally, while our findings may have important applications, we would like to point out

the modest nature of our results. The remaining open issues are extensive, with the most striking and presumably difficult issue being the development of an organized approach to deriving the most efficient precursors based on limited spatio-temporal information for a high dimensional dynamical system. In contrast, here we address the issue of predictability in the context of several fixed prescribed precursors used in isolation.

II. MODELS

We focus on a set of models that have been suggested as possible dynamical analogs of seismic phenomena, which are described briefly below. We refer to the models as the Bak, Tang, and Wiesenfeld (BTW) model [1], the Olami, Feder, and Christensen (OFC) model [2], the Chen, Bak, and Obukov (CBO) model [3], and the Uniform Burridge and Knopoff (UBK) model [4,7]. More detailed descriptions of the individual models may be found in the references cited above.

We begin with the UBK model, which satisfies a nonlinear wave equation

$$\frac{\partial^2 U}{\partial t^2}=\frac{\partial^2 U}{\partial x^2}-U-\phi(\dot{U})+vt \ . \tag{1}$$

Here $U(x,t)$ represents the relative displacement of opposite sides of a homogeneous fault as a function of position x and time t. The variable v is the very slow uniform shear rate driving the relative motion of the plates, and the key instability leading to chaotic behavior is a velocity-weakening, stick-slip friction law $\phi(\dot{U})$:

$$\phi(\dot{U})=\begin{cases}(-\infty,1] \ , & \dot{U}=0 \\ \dfrac{(1-\sigma)}{1+[2\alpha\dot{U}/(1-\sigma)]} \ , & \dot{U}>0 \ .\end{cases} \tag{2}$$

We numerically integrate this equation in the finite-difference approximation, in which the system can be thought of as a one-dimensional chain of blocks that is pulled slowly across a rough surface. Each block is connected to its nearest neighbors by springs [the Laplacian term in (1)] which represent linear elastic compressional forces along the fault. Each block also experiences a linear elastic shear force [the linear restoring force in (1)] modeled by a spring, which connects the block to a fixed point on one side of the fault. A block begins to slip—initiating an earthquake—when the sum of the shear and compressional forces exceeds the static friction threshold specified by $\phi_{\max}(\dot{U}=0)=1$. We include the "onset parameter" σ in the friction law so that we can study the limit of infinitesimal driving rates $v\to 0$, which leads to a clear separation between the time scale on which the system is loaded and the much shorter time scale on which individual events take place.

Unlike the UBK model, all of the other models ignore the details of inertial dynamics and friction laws and instead evolve according to specified "breaking rules," so that when the stress of a local block exceeds a threshold it relaxes according to some avalanche dynamics. For each of these the system can be thought of as a two-dimensional [8] square lattice of $(N\times N)$ "blocks" with open boundary conditions. In each case there is a particular rule which specifies the stress drop of the toppling site, the increases in stress of other sites, and the net stress drop of the system.

The BTW model is the original sandpile cellular automaton. Of those we are considering, it is the only model that is driven stochastically: on each iteration of the automaton the stress of a randomly selected site is increased by unity. If that site is above a specified threshold stress it initiates an avalanche in which each toppling site loses four units of stress, giving one unit to each neighbor (stress is dissipated at the boundary). This is represented by the following set of rules.

$$\begin{aligned}&\text{Driving}: \ h(i,j)\to h(i,j)+1 \ , \ \ i,j\in(1,N) \ , \ \text{random} \ ; \\ &\text{toppling} \ (h(i,j)\geq h_c): \ h(i,j)\to h(i,j)-4 \ , \\ &\qquad\qquad h(i\pm 1,j)\to h(i\pm 1,j)+1 \ , \\ &\qquad\qquad h(i,j\pm 1)\to h(i,j\pm 1)+1 \ ; \\ &\text{boundary conditions}: \ h(i,N+1)=h(i,0)=0 \ , \\ &\qquad\qquad h(N+1,j)=h(0,j)=0 \ .\end{aligned} \tag{3}$$

In the above, $h(i,j)$ is the sandpile height at site (i,j). An avalanche is considered over when all sites are below threshold.

In the OFC and CBO models (as in the UBK model) stress is increased uniformly across the whole system. The OFC model is similar to the BTW model in that equal stress is transferred to each neighbor in each toppling. However, unlike the BTW model, in the OFC model the internal dynamics does not conserve stress. Instead, in each toppling the stress of the toppling site is set to zero, and each neighbor receives a fraction $\alpha<0.25$ of the initial stress of the toppling site (we will typically take $\alpha=0.2$). Any remaining stress is dissipated.

The OFC model is intended to represent a cellular automaton realization of a two-dimensional Burridge-Knopoff model with a simpler friction law than that taken above in the UBK model. In the OFC model springs with constants K_L characterize the linear elastic shear restoring force, and coupling springs with constants K_1 and K_2 characterize the linear elastic response to longitudinal and transverse deformations in the plane of the fault. Here we consider the isotropic case in which $K_1=K_2\equiv K_C$. The stress on site (i,j) is given by $F_{i,j}=K_C(2x_{i,j}-x_{i-1,j}-x_{i+1,j})+K_C(2x_{i,j}-x_{i,j-1}-x_{i,j+1})+K_L x_{i,j}$, in which $x_{i,j}$ is the displacement of the block at site (i,j) from its equilibrium position. Given these definitions, the model is then updated as follows.

$$\begin{aligned}&\text{Driving (uniform)}: \ \propto K_L V \ , \ \text{in the limit} \ V\to 0 \ ; \\ &\text{toppling} \ (F_{i,j}>F^{th}): \ F_{i,j}\to 0 \ , \\ &\qquad\qquad F_{i\pm 1,j}\to F_{i\pm 1,j}+\delta F_{i\pm 1,j} \ , \\ &\qquad\qquad F_{i,j\pm 1}\to F_{i,j\pm 1}+\delta F_{i,j\pm 1} \ ; \\ &\text{boundary conditions}: \ F_{i,N+1}=F_{i,0}=0 \ , \\ &\qquad\qquad F_{N+1,j}=F_{0,j}=0 \ ,\end{aligned} \tag{4}$$

where V is the relative plate velocity and

$$\delta F_{i,j\pm1}=\delta F_{i\pm1,j}=\frac{K_C}{4K_C+K_L}F_{i,j}\equiv\alpha F_{i,j}\ , \tag{5}$$

which defines the parameter α. This model has received considerable attention as a possible nonconservative example of SOC, although there has been some debate over whether this model exhibits SOC in the thermodynamic limit [9].

Among the models we are considering, the CBO model is unique in that it is the only one in which the relaxation dynamics explicitly takes place using long-range interactions, rather than by redistributing stress only to neighboring sites. Like the BTW model, the CBO model does conserve stress away from the boundary. However, due to the long-range interactions, for any finite system stress is not conserved during any event, with breaking sites which are closer to the boundary dissipating more than interior sites. In addition, while it is not driven stochastically, it does contain a stochastic element—after each site topples, its threshold stress is reset to a random value chosen uniformly from [0,1]. In contrast, all of the other models have a fixed uniform threshold. Physically, the equations represent a square lattice of blocks, each of which is coupled to its nearest neighbors by springs. The shear stress is increased in, for example, the y direction until one of the springs breaks. The stress of the toppling site is set to zero and the stress redistribution over the rest of lattice is that due to a dipole force at the toppling site (thus falling off as r^{-d}). Specifically, if the stress in the spring between site $\mathbf{r}=n_x\mathbf{e}_x+n_y\mathbf{e}_y$ and $\mathbf{r}+\mathbf{e}_i$ is denoted $\sigma_i(\mathbf{r}),i\in\{x,y\}$, then the model is defined by the following rules:

$$\begin{aligned}
&\text{Driving}: \quad \sigma_y(\mathbf{r})\to\sigma_y(\mathbf{r})+p\ , \quad \text{uniformly with } p\to 0\ ;\\
&\text{toppling } [\,|\sigma_i(\mathbf{r}_0)\equiv\sigma_0|>\sigma_i^{th}(\mathbf{r}_0)\,]: \quad \sigma_i(\mathbf{r}_0)\to\sigma_i(\mathbf{r}_0)-\sigma_0\ ,\\
&\qquad\qquad \sigma_i^{th}(\mathbf{r}_0)\to\sigma_i^{th}(\mathbf{r}_0)\in[0,1]\ , \quad \text{breaking spring}\ ;\\
&\qquad\qquad \sigma_i(\mathbf{r})\to\sigma_i(\mathbf{r})+\sigma_0(G_i(\mathbf{r}-\mathbf{r}_0)-G_i(\mathbf{r}-(\mathbf{r}_0+\mathbf{e}_i))\ , \quad \text{other springs}\ ,\\
&\text{boundary conditions}: \quad \sigma_i(\mathbf{r})=0\ , \quad n_x,n_y\notin(0,N)\ .
\end{aligned} \tag{6}$$

Here $G_i(\mathbf{r})$ are the lattice dipole Green's functions which determine the change in stress for the springs representing shear ($i=y$) and axial ($i=x$) forces. That is, they are solutions to the lattice difference equations, involving both the vertical and horizontal spring stresses, which express the conditions that the earth be at rest between events (zero net force on each block due to its neighbors) and undergo linear elastic deformations away from the rupture (Hooke's law springs) [3].

While the BTW, OFC, and CBO models clearly differ from one another in certain important ways, at least for the system sizes considered here they all generate pure power-law event size distributions,

$$P(s)=s^{-(b+1)}\ , \tag{7}$$

(see Fig. 1), analogous to the Gutenberg-Richter law [5] describing seismicity catalogs taken from the entire earth or large regional fault systems. Thus we will refer to these systems as examples of SOC, with emphasis on "criticality" because the power law extends from the smallest event size up to essentially the system size.

In contrast, the UBK model, while self-organizing, is not critical. The event size distribution consists of a power law describing the small to moderate events, and excess large events, which cut off at some characteristic size, independent of the system size [10] for systems which are large enough (Fig. 1). This statistical distribution is analogous to what is thought to apply to individual faults, or narrow fault zones, where the largest events appear to dominate the total slip, occurring at a rate which exceeds the extrapolated rate of small to moderate events [11,12].

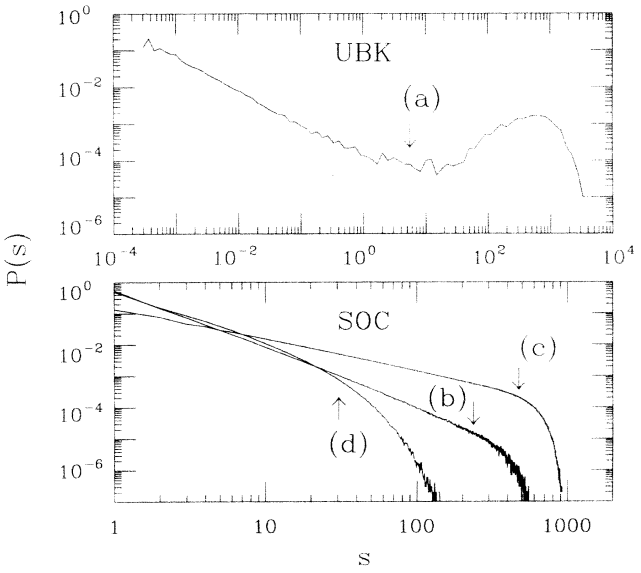

FIG. 1. Event size distributions $P(s)$ vs s for the (a) UBK, (b) OFC, (c) BTW, and (d) CBO models. In each case s is a measure of the size of the event—the integrated slip (seismic moment) for the UBK model, and the number of sites which topple for the others. In each case we attempt to predict events with $s\geq\bar{s}$, where $\bar{s}$ is some characteristic size (in each case $\bar{s}$ is marked with an arrow). The UBK model exhibits a sharp distinction between small ($s<\bar{s}$) and large ($s\geq\bar{s}$) events, while the others exhibit power laws cut off at $s\approx\bar{s}$ (determined by finite size effects). In these cases, to exactly determine this crossover length a careful study of finite size effects must be performed. For the purposes of qualitative comparisons, it is sufficient to roughly estimate $\bar{s}$ as we do here. We take $N=8192$, $\sigma=0.01$, $\alpha=3$, and $\xi/a=10$ for the UBK model [1], system sizes 32×32 for the other models, and $\alpha=0.2$ for the OFC model [2].

III. PREDICTION ALGORITHM

Our method of forecasting resembles the algorithm M8 introduced by Keilis-Borok and Kossobokov [6], which is currently being studied as a possible means of using worldwide seismic data sets to predict the largest earthquakes in any given region. The M8 algorithm is based on the hypothesis that regional small scale seismicity may be used to diagnose an upcoming large event. The procedure is to first coarse grain the catalogs in space and time, and then to measure certain precursors in these space-time windows. In particular, in the earth, seismogenic zones are divided into overlapping circles $\Delta\mathbf{x}$ with diameters (typically hundreds of kilometers) that are an order of magnitude larger than the size of the large event to be predicted. Each precursor is monitored separately within each circle for successive overlapping time intervals of length Δt. Together $\Delta\mathbf{x}$ and Δt define a space-time window $R \equiv (\Delta\mathbf{x}, \Delta t)$. The precursor values are updated every six months, and most of the precursors are evaluated on the basis of data accumulated over the full six year time window, which is still much shorter than the mean large event recurrence interval in the region (typically hundreds of years). Several precursors are used and include a variety of measures based on the activity A, which within each space-time window R is defined to be

$$A = \sum_{\text{events } i \text{ in } R} \theta(M_i - M_0) \, . \tag{8}$$

Here M_i is the magnitude (a logarithmic measure of the event size) of event i, M_0 is a lower magnitude cutoff, which is part of the definition of the precursor, and $\theta(x)$ is the unit step function. In words, A is the number of earthquakes within the space-time region that are identified as main shocks [13] and are greater than or equal to some threshold size. Note that A is easily deduced from the time series of events in a region, and large values of A indicate a regional temporal clustering of events. More generally, an effective precursor is one which will typically sustain elevated (or depressed) values prior to a large event relative to its average value.

In the earth no single measure has yet been identified which reliably predicts all of the large events. Instead the M8 algorithm combines seven different precursors in a voting algorithm which is used to make predictions. It is important to articulate the prediction goal defined by Keilis-Borok and Kossobokov. Instead of assigning some probability for an event to occur at a specific place and time in the future, the idea is simply to recognize certain seismicity patterns, i.e., sets of individual precursors that systematically exhibit elevated or depressed values prior to a large event, which might indicate a *time of increased probability,* or "TIP," for a large earthquake within the spatial region $\Delta\mathbf{x}$. In particular, if a fixed number, say T, of the precursors exceeds individual thresholds in a region, then the TIP is turned on. That is, if $f_j(R)$ is the value of the j^{th} precursor in space-time region R, and F_j^{th} is the precursor function threshold, then a TIP is declared in R when

$$T \leq \sum_{j \text{ precursors}} \theta[f_j(R) - F_j^{th}] \, . \tag{9}$$

This defines the voting algorithm. A TIP may be turned off either when a large event occurs or when the number of precursors exceeding their individual thresholds falls below the TIP threshold T.

The earliest applications of these methods were based on existing data in real catalogs, and it was found that in order to capture roughly 80% of the large events, approximately 20% of the total space-time volume had to sustain TIP's. Efforts are currently underway to evaluate the algorithms more thoroughly by establishing systematic tests for forward prediction [14]. However, use of the algorithm has been controversial for a variety of reasons, including the intrinsic sensitivity to the inherent inaccuracies and incompleteness of the catalogs [15] and sensitivity of the algorithm to features such as the initial placement of test regions (the space-time windows), where small adjustments in the spatial positions of the regions and start dates of the catalogs can easily cause the algorithm to miss some of the events [16]. Of course, given a perfectly accurate catalog of arbitrary length (such as can easily be generated for models), the performance of these algorithms could easily be assessed. However, such catalogs are simply not available, so that the question of the predictability of earthquakes, as well as the development of effective algorithms, remain open and active areas of research. Here we will assess how well similar algorithms can be made to work on a collection of dynamical models.

We consider a simplified version of this prediction algorithm, in which precursors are considered individually. We turn a TIP on when the precursor exceeds its individual threshold and turn the TIP off when the precursor falls below the threshold. By varying the threshold we vary the total alarm time and from this we construct a *success curve* [17] which plots the fraction of events predicted as a function of the fraction of the total space-time volume occupied by TIP's. Thus each precursor threshold value generates a single point along the success curve. (All of our thresholds are integer values, hence the figures show a linear interpolation between the actual data points.)

Comparison of the success curves allows us to compare the effectiveness of different precursors as well as the predictability (based on these precursors) of different models. For a simple null test, our results can also be compared with the corresponding results for purely random methods, in which TIP's are issued completely arbitrarily. In that case, events are predicted purely by chance and the fraction which are predicted successfully is simply given by the fraction of time the TIP is on: (% predicted)=(% alarm time), i.e., the success curve is the diagonal line. In a purely random system no algorithm will perform better than this method. In our case, this gives us an operational definition of predictability of models using a particular algorithm; if a model is predictable, the success curve for some precursor should deviate from this line in a statistically significant manner.

It is not necessary for the success curve to lie above the diagonal line. In principal, the curve could cross the line

or even lie completely below it. Any deviation from the diagonal is a sign that the precursor is detecting some correlation (or anticorrelation) in the system. However, because of the way the algorithm is defined in practice to obtain a success rate which is better, rather than worse, than the corresponding results for random methods, one must base predictions on the complement of the original precursor whenever the success curve lies below the diagonal line [18]. Note that in this case the precursor function will tend to exhibit depressed values prior to large events, so that the complement of this measure will exhibit increased values. For example, for activity A the complement $\overline{A}$ is lack of activity, defined in terms of A by choosing $\overline{F}^{th} = -F^{th} < 0$ and $\overline{A} = -A$.

Finally, because of the limited amount of data which is available in seismic catalogs, it is important to accompany any prediction with an assessment of the associated confidence level. In contrast, in our case we can generate catalogs that are arbitrarily long and thus obtain results to an arbitrarily high level of precision. In particular, to verify that our success curves have converged to their asymptotic limits in time, we generate independent curves for a series of exponentially growing time intervals. This ability to check for systematic convergence is especially useful for models in which the predictably is marginal.

IV. RESULTS

We begin with the UBK model. A small segment of the catalog of events is illustrated in Fig. 2. For each event, a line is drawn through all the blocks which slip. While precursory small scale seismicity is clearly correlated with the epicenters of future large events (much more so for the model than for the earth) [19] it begins on average after half of the mean recurrence interval between large events has elapsed, so that from Fig. 3 along it is not clear how accurate predictions based on this pattern will be.

In Ref. [20] a detailed study of predictability of the UBK model revealed that among a set of precursors, the two most effective are activity A which is the number of earthquakes and a new measure which is a better measure of the development of spatial correlations. This new measure, which we call active zone size S_{AZ}, is the number of blocks which have slipped (independent of the number of times) in some event contained within the current space-time window. Equivalently,

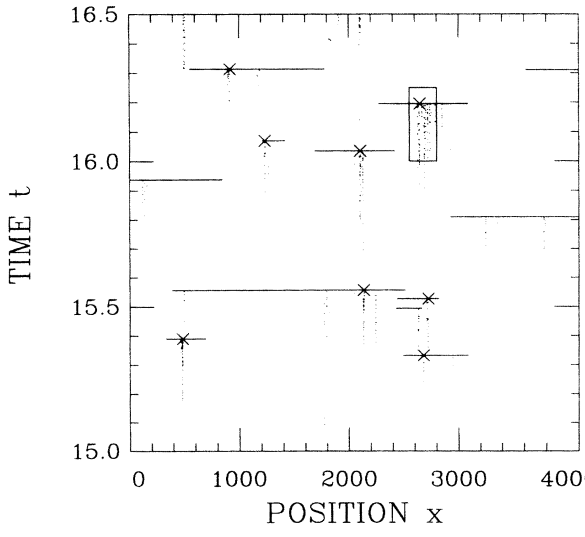

FIG. 2. A small sample catalog as a function of space x (block number) and time t in the UBK model. A line segment marks blocks which slip in each event, and a cross marks the epicenter of each large event, which is clearly correlated with the small scale seismicity. The box corresponds to a space-time window within which A and S_{AZ} are evaluated. Time is measured in units of the inverse loading speed v^{-1}.

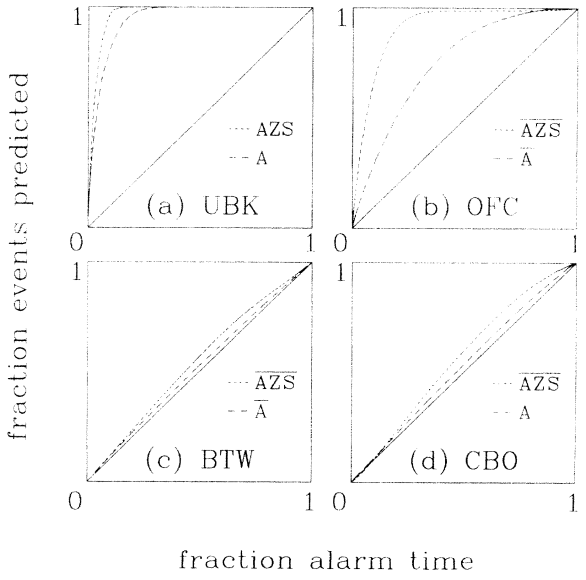

FIG. 3. Success curves for the (a) UBK, (b) OFC, (c) BTW, and (d) CBO models. For each model, the best spatial measure (S_{AZ} or $\overline{S}_{AZ}$) leads to more precise predictions than the best temporal measure (A or $\overline{A}$). In each case, results for the complement measure (e.g., A vs $\overline{A}$) are obtained by a refection of the curve across the diagonal. In the UBK model, we predict epicenters of large events and optimal spatial windows are less than the size of the large event as shown in Fig. 3. We coarse grain the system into many overlapping spatial regions, and then obtain the success curve by calculating the fraction of events successfully predicted by some window containing the event vs the total fraction of the space-time volume which is occupied by TIP's [3]. In the other models, the spatial windows are taken to be the entire system and the goal is to predict the large event. We have performed a crude optimization to select the time windows within which the precursors are evaluated. The values correspond to $\Delta t = 0.1$ for the UBK model (where the spatial windows were taken to be 213 blocks), 33 net grains added during the time window for the BTW model, 0.15 net stress added per site for the OFC model, and 0.007 net stress added per site in the measurement of $\overline{S}_{AZ}$ and 0.015 net stress added per site in the measurement of A for the CBO model.

$$S_{AZ} \equiv \sum_{\text{sites } k \in \Delta x} \delta(k-k') \ , \quad k' \in \text{ some event } M_i \text{ in } R \ . \tag{10}$$

With A we are able to predict 90% of the large events, with alarms occupying 15% of the total space-time volume (Fig. 3), which corresponds to alarms which occupy significantly smaller time intervals than the average duration of small scale seismicity prior to large events [20] in Fig. 2. However, the performance of S_{AZ} is even more impressive, leading to successful predictions of 90% of the large events when alarms occupy only 8% of the space-time volume [21]. In the UBK model the effectiveness of S_{AZ} can be traced to the fact that very little stress is relieved when a block slips in a small event. Instead, small events serve as markers that the region is locally close to threshold. While the two precursors are clearly not independent, in contrast to A, S_{AZ} is a much more direct measure of the size of the region that is near the threshold for slipping and thus ultimately leads to the more direct assessment of the probability of a large event.

The question remains as to which precursors that worked well for the UBK model are effective precursors for other self-organizing systems. To address this, we next consider the SOC models. Apart from some measurements of correlation functions between events of similar size in the OFC model [22] (which detected a tendency or large events to cluster in time) there has been little work to characterize the SOC models in terms of the predictability.

As previously noted, the behavior of the UBK and SOC models differ from one another substantially. In principle, for the SOC models we could coarse grain the catalogs of events in space and time in a manner exactly like that used for the UBK model. However, because in the SOC models the largest events span essentially the entire system and it is these largest events we wish to forecast, the most sensible choice is to define the spatial windows to correspond to the entire system. Furthermore, in these systems the distinction between small precursory events and the large events which we attempt to predict is no longer a sharp feature, as is apparent in the statistical distributions. For that reason, we set a somewhat arbitrary lower cutoff for events we wish to predict, which corresponds to the size where we estimate (by eye) that finite size effects first become apparent (see Fig. 1). Our preliminary estimates of the predictability of small and medium size events indicate that in comparison the largest events are at least as predictable, and in most cases significantly more so, than the others [23].

The success curves for the SOC models, as well as our previous results for the UBK model, are illustrated in Fig. 3. For all of the models, both A and S_{AZ} yield success curves that deviate systematically from the results obtained for random methods (the diagonal line) and thus lead to some measurable predictability. In each case along essentially the entire success curve, S_{AZ} gives the greater deviation and hence is more effective than A as a precursor for a coming large event. For the SOC models, we find that in most cases these measures are in fact anticorrelated with large events, with success curves falling below the diagonal. Whenever this is the case, we plot the complements of these measurers, i.e., lack of activity $\overline{A}$ (quiescence) and lack of the active zone size $\overline{S}_{AZ}$ because these are the measures which would be used in practice to obtain a success rate which is better than random methods. Of the SOC models, the OFC model is clearly most predictable, generating a success curve which is comparable to that of the UBK model. In this case the most effective measure is $\overline{S}_{AZ}$, leading to 90% events predicted with alarm times of order 20%. Similarly, for the BTW and CBO models, $\overline{S}_{AZ}$ outperforms measures based solely on activity ($\overline{A}$ for the BTW model, and A for the CBO model). However, compared to the UBK and OFC models, the gain over purely random methods is significantly reduced.

In each case there is at least some correlation between small scale activity and coming large events, suggesting (but by no means proving) that self-organization may have implications for the predictability of real systems [24]. The poor performance in the BTW and CBO models indicates that the correlations need not be strong and may in real systems be sufficiently weak that external noise or limited statistics may mask their presence. Recall that both the BTW and CBO models contain stochastic attributes, which we expect play important roles in limiting their predictability. In contrast, both the UBK and OFC models, which exhibit the highest levels of predictability, are fully deterministic. However, the UBK and OFC models have an additional common feature, which differentiates them from the BTW and CBO models. Both the UBK and OFC models do not satisfy a conservation law in the redistribution of internal stress. A more detailed study is necessary to fully separate the relative roles of deterministic dynamics and the lack of conservation in defining the predictability of different systems, even within our limited definition of predictability. However, to address this question at least in part we have considered the predictability of the OFC model as the conservation parameter is varied. In that case we find that the predictability diminishes systematically as the level of conservation is increased, although, as illustrated in Fig. 4, even when the OFC model is fully conservative its predictability is clearly greater than that illustrated in Fig. 3 for the BTW and CBO models [22,23].

In the SOC models the precursors based on quiescence are typically most effective because, unlike the UBK model, the stress on a site is set to zero each time a block slips, independent of the even size. Thus a lack of events is more likely to signify that the system is near the slipping threshold. Interestingly, in the earth both increases and decreases of seismicity have been observed prior to large events [25], suggesting that perhaps the UBK and SOC models may all contain some elements which are relevant to real faults. Ultimately, it may be of interest to incorporate the more complete dynamical treatment of individual faults present in the UBK model into an SOC-type model which describes fault zones.

In both the UBK and SOC models, large events involve large spatial regions, so that in order for a large event to occur, the system must be near threshold across a rela-

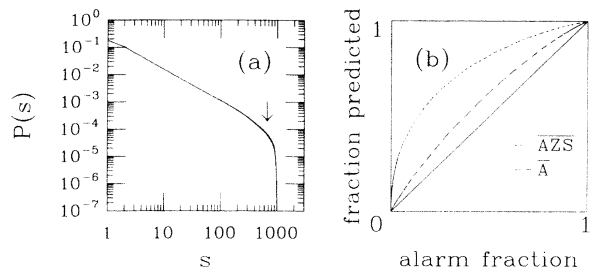

FIG. 4. The deterministic and fully conservative OFC model. Here $\alpha=0.25$, whereas the results presented in Figs. 1 and 3 correspond to the dissipative case $\alpha=0.2$ (a) illustrates the event size distribution, with $\bar{s}$ marked as in Fig. 1, and (b) illustrates the success curve, analogous to Fig. 3. Compared to the nonconservative case [Fig. 1(b)], here the maximum event size is significantly increased, and compared to Fig. 3(b) the predictability is suppressed. As in Fig. 3, here we have crudely optimized over time windows to select a window which corresponds to 0.05 net stress added per site.

tively large region in space. In all of the models considered here, thresholds based on S_{AZ} are more effective than those based on A, since S_{AZ} provides the more direct measure of the development of such regions. The strong performance of this new precursor is particularly noteworthy because such measures are not currently being used quantitatively in earthquake prediction algorithms such as M8. Certain tendencies towards clustering in space and time have been noted [26] and are the phenomenological basis of these algorithms. However, the precursors which are used are based on measures such as A which, within a given region, track the development of temporal correlations. In such measures, spatial correlations are only accounted for in the most primitive way, i.e., in the initial definition of the spatial window. In the earth, including precursors which measure the development of geometric spatial correlation is complicated by the inhomogeneity of fault networks and the difficulties associated with accurately locating slip. Nonetheless, a box counting algorithm, in which the current spatial windows are coarse grained and a count is made of regions exhibiting seismicity above or below some background level, may be adequate to measure the analog of S_{AZ} or $\bar{S}_{AZ}$. It would be of significant interest to assess the performance of such a measure in comparison to activity based precursors in the earth.

ACKNOWLEDGMENTS

We thank Volodya Kossobokov, James Langer, and Glen Swindle for useful comments on the manuscript. This work was supported by the Alfred P. Sloan and David and Lucile Packard Foundations, NSF Grant No. DMR-9212396, and an INCOR grant from LANL.

[1] P. Bak, C. Tang, and K. Wiesenfeld, Phys. Rev. Lett. **59**, 381 (1987).
[2] Z. Olami, H. Feder, and K. Christensen, Phys. Rev. Lett. **68**, 1244 (1992).
[3] K. Chen, P. Bak, and S. Obukov, Phys. Rev. A **43**, 625 (1991).
[4] J. Carlson and J. Langer, Phys. Rev. Lett. **62**, 2632 (1989).
[5] B. Gutenbrg and C. Richter, *Seismicity of the Earth and Related Phenomena* (Princeton University Press, Princeton, NJ, 1954).
[6] V. Keilis-Borok and V. Kossobokov, Phys. Earth Planet. Inter. **61**, 73 (1990).
[7] R. Burridge and L. Knopoff, Bull. Seismol. Soc. Am. **57**, 3411 (1967).
[8] The two-dimensional UBK model differs little from the one-dimensional case. J. Carlson, Phys. Rev. A **44**, 6226 (1991).
[9] J. Socolar, G. Grinstein, and C. Jayaprakash, Phys. Rev. E **47**, 2366 (1993).
[10] J. Carlson, J. Langer, B. Shaw, and C. Tang, Phys. Rev. A **44**, 884 (1991).
[11] See, e.g., D. P. Schwartz and K. J. Coppersmith, J. Geophys. Res. **89**, 5681 (1984).
[12] C. Scholz, *The Mechanics of Earthquakes and Faulting* (Cambridge University Press, New York, 1990).
[13] A main shock is defined to be the largest event in a sequence of earthquakes, consisting of a main shock followed by after shocks, and possibly preceded by foreshocks. Various different algorithms exist for associating aftershocks with a particular main shock in terms of their relative separation in space and time from the main shock. While one of the most prominent phenomena associated with real earthquakes is their tendency to generate long sequences of aftershocks, unfortunately we cannot consider aftershocks in this study because none of the models contains the time scales associated with aftershock sequences.
[14] J. Healy, V. Kossobokov, and J. Dewey, U.S. Geological Survey Open File Rep. No. 92-401 (1992).
[15] R. E. Habermann, Tectonophysics **193**, 277 (1991).
[16] J.-B. Minster and N. P. Williams, EOS Trans. **73**, 366 (1992).
[17] G. M. Mochan, Tectonophysics **193**, 267 (1991).
[18] A combination of the original measure and the complement measure will be most effective near places where the success curve crosses the diagonal line.
[19] B. Shaw, J. Carlson, and J. Langer, J. Geophys. Res. **97**, 479 (1992).
[20] S. Pepke, J. Carlson, and B. Shaw, J. Geophys. Res. (to be published).
[21] This method of obtaining the success curve for the UBK model differs from that used in Ref. [20] where success curves were obtained individually for each of the spatial regions, and then averaged to obtain the cumulative results. Here we consider alarms as they apply to the total space-time volume to obtain a somewhat more direct comparison to the SOC models.
[22] K. Christensen and Z. Olami, J. Geophys. Res. **97**, 8729 (1992).
[23] Issues associated with optimization will be discussed more fully in S. Pepke and J. Carlson (unpublished).
[24] K. O'Brian and M. Weissman, Phys. Rev. A **46**, R4475 (1992).
[25] H. Kanamori, *Earthquake Prediction, an International Review,* Maurice Ewing Series Vol. 4 (American Geological Union, Washington, DC, 1981), pp. 1–9.
[26] Y. Y. Kagan, Geophys. J. R. Astron. Soc. **71**, 659 (1982).